Journal of Materials Chemistry C



PAPER

View Article Online
View Journal | View Issue



Cite this: *J. Mater. Chem. C*, 2016 4. 5248

Wavelength-dependent optical transition mechanisms for light-harvesting of perovskite MAPbI₃ solar cells using first-principles calculations†

Hsin-An Chen, Ming-Hsien Leeb and Chun-Wei Chen*ac

The recently emerging class of solid-state hybrid organic—inorganic perovskite-based solar cells has demonstrated remarkably high power conversion efficiencies of up to ~20%. It is expected that a detailed understanding of wavelength-(or energy-)dependent optical transition processes for light harvesting of perovskite solar cell materials will be a crucial factor to further improve the photovoltaic performances. In this work, we would like to employ the first-principles calculations to investigate the wavelength-(or energy-)dependent optical transition mechanism for light harvesting of the CH₃NH₃Pbl₃ perovskite material. A method called the band-resolved optical constant analysis technique was developed to investigate the wavelength-(or energy-)dependent optical absorption mechanism of the perovskite material. Based on the analyses, we are able to visualize and quantize the detailed wavelength-(or energy-)dependent optical transition processes involved in the broad absorption spectrum of a perovskite material, which provides deep insight into the understanding of the light-harvesting mechanism of this promising photovoltaic material.

Received 23rd February 2016, Accepted 22nd April 2016

DOI: 10.1039/c6tc00773b

www.rsc.org/MaterialsC

Introduction

A recently emerging class of solid-state hybrid organic–inorganic perovskite-based solar cells, $^{1-3}$ evolving from the conventional DSSCs, has demonstrated remarkably high power conversion efficiencies of up to $\sim 20\%$, because of the superior physical properties of perovskite materials, such as high optical absorption coefficients, 4,5 low binding energies and long and balanced electron–hole diffusion lengths. $^{6-8}$ A basic requirement of a photovoltaic material is that it first generates free charge carriers produced by photoexcitation. Subsequently, these carriers are transported through the device to the electrodes without recombining with oppositely charged carriers or traps, and are collected by two opposite electrodes. Most state-of-the-art perovskite solar cells typically consist of a device structure based on a mesoporous metal oxide scaffold, on which the organometal halide perovskites such as $CH_3NH_3PbX_3$ (X = Cl, Br, I) as light-harvesting materials

are grown, followed by the deposition of a hole transport layer.² The most intriguing feature of high-performance organicinorganic hybrid perovskites is that they consist of long-range balanced electron-hole diffusion lengths⁷ and they can support both electron and hole transport, exhibiting ambipolar transport behavior. Many photocarrier dynamics experiments have been performed to explore the carrier relaxation and transport of perovskite materials. 9-11 Because the perovskite photovoltaic materials have a wide range of absorption spectra which matches well with the solar spectrum, 12-14 both electron and hole extraction efficiencies of perovskite materials were found to strongly depend on the related energy levels of these optical absorption states to those of the collecting electrodes. For example, the transient absorption spectroscopy revealed that the carrier relaxation dynamics at two distinct linear absorption peaks located at 480 nm and 760 nm show quite different charge transfer behaviors.⁹ It will be expected that the understanding of wavelength(or energy)-dependent optical transition processes for light harvesting of perovskite solar cell materials will be of great importance to achieve a further improvement in the photovoltaic performances. In this work, we would like to employ the first-principles calculations to investigate the wavelength-(or energy-)dependent optical transition mechanism for light harvesting of CH3NH3PbI3 perovskite material as shown in Fig. 1(a). Because optical absorption mechanisms in solid-state materials typically involve complicated transition processes between occupied and unoccupied bands in

^a Department of Materials Science and Engineering, National Taiwan University, No.1, Sec. 4, Roosevelt Rd., Da-An Dist., Taipei City 10617, Taiwan. E-mail: chunwei@ntu.edu.tw

^b Department of Physics, Tamkang University, No.151, Yingzhuan Rd., Tamsui Dist., New Taipei City 25137, Taiwan

^c Taiwan Consortium of Emergent Crystalline Materials (TCECM), Ministry of Science and Technology, Taiwan

 $[\]dagger$ Electronic supplementary information (ESI) available: Details of partial density of states and analyses, and the absorption spectrum. See DOI: 10.1039/c6tc00773b

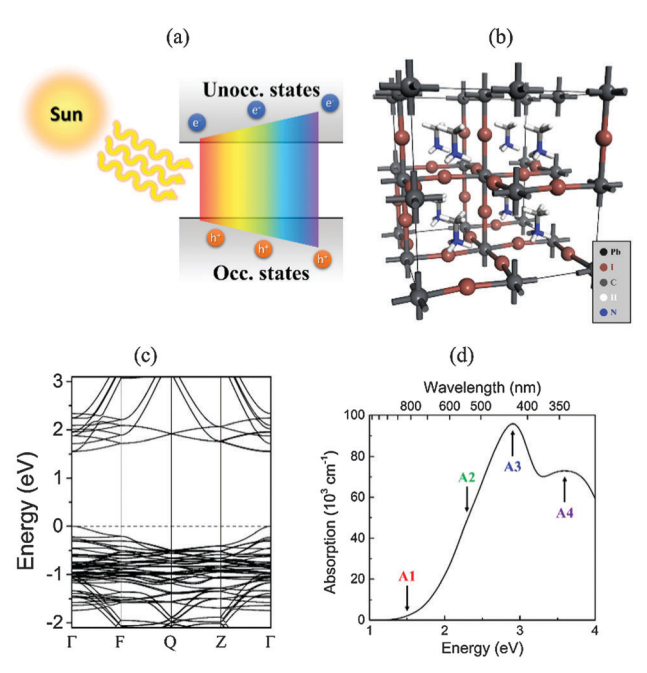


Fig. 1 (a) The schematic plot of the wavelength-dependent light harvesting of a perovskite-based material. (b) The crystal model and (c) the band structure and (d) the calculated optical absorption spectrum of the polar MAPbI₃

the corresponding band structure according to the selection rule, a method called the band-resolved optical constant analysis technique was developed to investigate the wavelength-(or energy-)dependent optical absorption mechanisms of perovskite materials at each sub-system which is mainly responsible for optical absorptions at individual photoexcited energies. Based on the analyses, we are able to visualize and quantize the detailed wavelength-(or energy-)dependent optical transition processes involved in the absorption spectrum of a perovskite material, which provides deep insight into the understanding of the lightharvesting mechanisms of this promising photovoltaic material. Moreover, the development of the band-resolved optical constant analysis technique can also be applied to reveal the complicated optical transition processes in other semiconductor materials.

The total energy and electronic structure calculations were performed using the CASTEP code, 15 which is a plane-wave, pseudopotential program based on the density functional theory (DFT). Generalized gradient approximation (GGA) was used with the exchange-correlation potential by Perdew, Burke and Ernzerhof (PBE).¹⁶ The ion-electron interaction was modelled by the ultrasoft pseudopotential.¹⁷ These models were constructed within a tetragonal supercell with the kinetic-energy cutoff being set to be 400 eV. The k-point sampling using a Monkhorst-Pack grid18 with a 0.025 Å-1 k-point spacing was used to ensure the convergence in calculations. Electronic structures were optimized with the maximum force of 0.01 eV \mathring{A}^{-1} . The aristotype of perovskite consists of a structure with a space group of ABX3, where the cation B occupies the octahedral site and is bonded to 6 X anions. Each [BX₆] octahedron is corner-shared with one another to form a three-dimensional framework with the cation A which occupies the central cuboctahedral site. 19 The organic-inorganic

hybrid compound CH₃NH₃PbI₃ (MAPbI₃) is a material consisting of a perovskite structure (ABX₃; A = MA, B = Pb, C = I), where the orientations of MA cations may result in some distortion of the ideal perovskite lattice. 17,18 At room temperature, the orientations of the MA cations have been reported to exhibit random distribution from the experimental result by X-ray diffraction. 20,21 In this work, we proposed two types of MAPbI3 structures to investigate the corresponding optical transition mechanisms for light harvesting; one is the polar perovskite structure (p-MAPbI₃) where all MA cations are aligned along the same direction and the other structure is the nonpolar perovskite structure (np-MAPbI₃) with no preferred orientation of MA cations. Fig. 1(b) shows the representative model of the p-MAPbI₃ which consists of a tetragonal lattice with all the MA cations aligned along the z axis. The calculated lattice parameters after relaxation are a = b = 9.01 Åand c = 13.11 Å. The corresponding band structure of the polar perovskite p-MAPbI₃ as shown in Fig. 1(c) exhibits a direct band gap 1.55 eV at the Γ point, which is similar to the previously calculated results^{20,22-25} and experimental results.^{22,26-28} The calculated band gap energy is not underestimated under the GGA-PBE scheme. The optical properties are calculated based on the independent-particle approximation, where the excitonic effects and the local-field corrections are neglected. Typically, the imaginary part of the dielectric function $\varepsilon_2(\omega)$ was first calculated using the usual perturbation-theory-derived sumover-states formalism,

$$\varepsilon_2(\omega) = \frac{4\pi^2}{\Omega \omega^2} \sum_{\substack{i \leq \text{VB} \\ k \neq 0}} \sum_k w_k |p_{ij}|^2 \delta(E_{kj} - E_{ki} - \omega), \tag{1}$$

where Ω is the unit cell volume, and ω is the photon energy. VB and CB denote the valence and conduction bands respectively. The p_{ii} denotes the momentum matrix elements obtained from the band structure calculations and w_k is the k-point weighting needed for the symmetric k-reduced sets. The real part of the dielectric function $\varepsilon_1(\omega)$ can be calculated by the Kramers-Kroing transformation.²⁹ All other linear optical properties such as the absorption coefficient and the refractive index can be obtained as functions of both the real and imaginary parts of the dielectric function. Fig. 1(d) shows the calculated linear absorption spectrum $\alpha(\omega)$ of p-MAPbI₃ as a function of incident photon energies. The onset photon absorption energy of polar MAPbI₃ is about 1.5 eV, which is close to its electronic band gap value. A gradual increase in absorption intensities with increased photon energies in the visible-light range was found, showing a good agreement with the absorption spectrum of the MAPbI₃ perovskitebased material obtained from the experimental result.30-32

Typically, the energy-dependent absorption coefficients $\alpha(\omega)$ is directly related to the optical constant of the imaginary part of the dielectric function $\varepsilon_2(\omega)$ of a material, where $\varepsilon_2(\omega)$ strongly depends on the dipole transition matrix elements p_{ii} resulting from optical transition processes from valence bands (VB) to conduction bands (CB) according to the selection rule. However, the detailed information on energy-dependent optical transition processes cannot be obtained solely from the calculated density of states (DOS) and band structure because the selection

rule and the corresponding dipole transition matrix elements need to be taken into account. In order to analyze the optical transition processes contributed to the dielectric function $\varepsilon_2(\omega)$ at each photon energy, the band-resolved optical constant analysis technique is thus developed by modifying the previously developed method on the non-linear optical properties of materials, $^{33-35}$ which allows us to analyze the corresponding optical transition processes for light-harvesting in MAPbI $_3$ at individual energy-dependent levels. The main idea of the band-resolved optical constant analysis technique is to obtain the effective dielectric function $\varepsilon_2(\omega)$ for each band through a "band-resolved" partial summing strategy.

Accordingly, the corresponding weighting factors for "occupied" or "unoccupied" bands, when normalized by the total imaginary part of the dielectric function $\varepsilon_2(\omega)$, can be obtained. Based on the scheme, the band-resolved $\varepsilon_{2,ik}^{\rm occ}(\omega)$ at the occupied band and $\varepsilon_{2,jk}^{\rm unocc}(\omega)$ at the unoccupied band can be obtained separately by fixing one occupied band index i or one unoccupied band index j, respectively, and the sum of the rest of the band indices in the double summation as described in eqn (1). Partial contributions of each ith for "occupied" or "unoccupied" bands can be expressed as $w_{\omega,jk}^{\rm occ} = \varepsilon_{ik}^{\rm occ}(\omega)/\varepsilon_2(\omega)$, which can be used as weighting factors to construct the corresponding occupied band (valence band) probability densities involved in the optical transition processes,

$$\rho_{\omega}^{\text{occ}}(r) = \sum_{k} \sum_{i=1}^{\text{occ}} w_{\omega,ik}^{\text{occ}} |\psi_{ik}(r)|^2 w_k$$
 (2)

 $\rho_{\omega}^{\rm occ}(r)$ corresponds to all the contributions from occupied bands to the total $\varepsilon_2(\omega)$ function at frequency ω , where $\psi_{ik}(r)$ is the wavefunction in the ith occupied band and at the k-point k, and w_k is the symmetry-reduced k weighting. The same scheme can also be applied to obtain the unoccupied band probability densities. Because both the weighting factors and the weighted densities are photon energy dependent, we are able to projectout the most important energy levels and orbitals which are predominantly responsible for the corresponding optical transition processes from the distributions of weighting factors and weighted densities. Such a weighted-density analysis scheme is thus used to visualize the three-dimensional optical transition processes attributed to the effective dielectric function $\varepsilon_2(\omega)$ at different energies, which may be directly correlated with the "absorption strength" throughout the entire space. The result represents the most important occupied (or unoccupied) electronic structure of the sub-systems that are mainly responsible for optical absorptions at individual photoexcited energies. Through the band-resolved optical constant analysis technique, both qualitative information (spatial distributions) and quantitative information (ratios of contributions) can be obtained to understand the wavelength-(or energy-)dependent optical transition mechanism.

Results and discussion

Fig. 2 shows the optical transition density (OTD) contour plots at the selected transition energies marked at Fig. 1(d) with 1.5 eV (A1), 2.3 eV (A2), 2.9 eV (A3) and 3.6 eV (A4), respectively, which denote

the total sum of all the orbital densities of the occupied and unoccupied bands including all the different k points contributing to the optical transition processes at the corresponding energies. The OTD plots clearly reveal the information on the atoms and orbitals at valence and conduction bands participating in the optical transition processes. It is found that all of these optical transition densities at occupied and unoccupied bands participating in the optical transition processes are mainly located at either Pb or I atoms within the lead tri-iodide framework accordingly. No state of MA cations was found to be involved in the optical transition in the visible-light region, which is consistent with the result of the partial density of states (PDOS) analysis (as shown in the ESI†). In addition, the corresponding orbital density distributions of the occupied and unoccupied bands at these four representative energies are quite different, indicating that the optical absorption processes at different energies of a perovskite material strongly depend on the orbital types of Pb and I atoms. Based on the band-resolved optical constant analysis, we are able to "visualize" the spatial distributions of orbital densities at each atom which involve in the optical transitions. Fig. 2 thus contains the information on the total sum of orbital densities from the occupied and unoccupied bands at different energies including all the k points, each of which consists of the combination of different types of optical transitions. In order to obtain more detailed information on the individual optical transition at each k point, the weighting scheme of the band-resolved optical constant analysis technique according to eqn (2) was further employed in the following section.

Fig. 3(a) shows the molecular orbital (MO) diagram of bonding configurations of Pb atoms and I atoms at the Γ point obtained from the calculated band structure and density of states. The occupied states near the Fermi energy are mainly attributed to interactions between the s orbitals of Pb atoms (Pb_s) and the p orbitals of I atoms (I_p) as shown schematically in the inset of Fig. 3(a). Three different energy states of VB1, VB2 and VB3 correspond to three bonding configurations. The VB1 and VB3 states correspond to the antibonding (denoted as σ^*) and bonding (denoted as σ) states, respectively, resulting from the interactions between Pb_s states (with octahedral hybridization) and I_p states (with linear hybridization) within the framework,

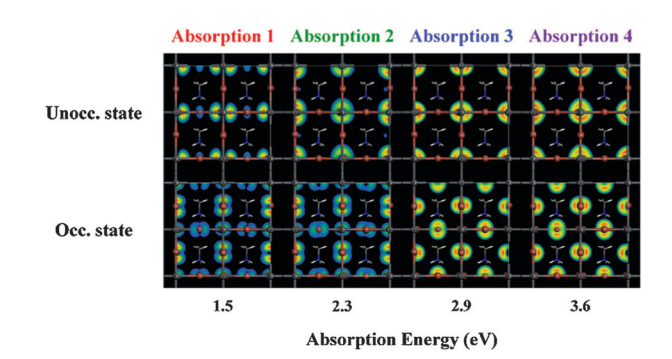


Fig. 2 The optical transition density (OTD) contour plots at the selected transition energies marked at Fig. 1(d) with 1.5 eV (A1), 2.3 eV (A2), 2.9 eV (A3) and 3.6 eV (A4), respectively.

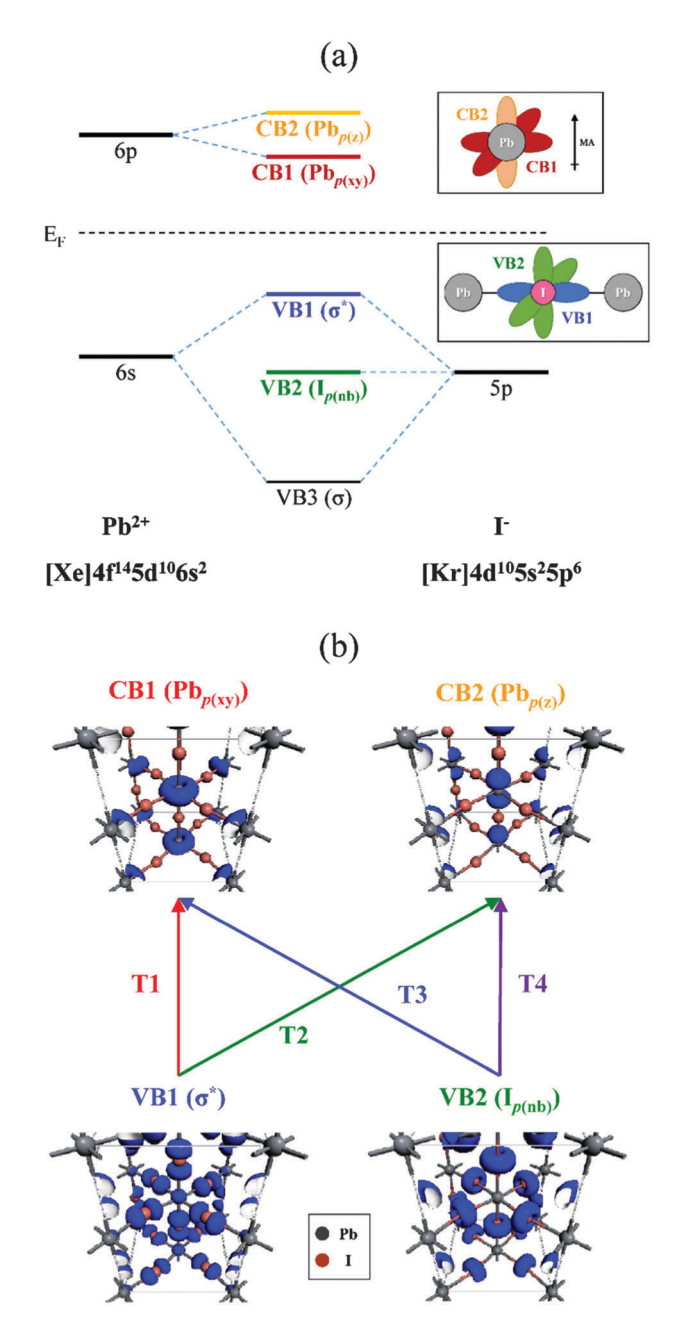


Fig. 3 (a) The MO diagram of the lead triiodide framework with inset schematic plots of bondings and orbitals of VBs and CBs. (b) The corresponding energy orbital densities related to the four predominant optical transition processes T1-T4 calculated at the Γ point.

whereas the VB2 corresponds to the non-bonding state of I_p (denoted as $I_{p(nb)}$) as a result of the off-axis p orbitals of I atoms without hybridization with Pb atoms. By contrast, the unoccupied states are mainly attributed to p orbitals of Pb atoms (Pbp states). For the polar MAPbI₃, the structure consists of a tetragonal lattice with well-aligned MA cations along the z axis, leading to different lattice distortions along the z axis (vertical direction) and x-y axes (horizontal direction). Different bond lengths of Pb-I bonds could be observed in the framework, where the bond lengths in the vertical direction (the z axis) are longer than those in the horizontal direction (x and y axes). Hence the Pb_p states,

which were originally degenerate in Pb atoms, would be split into the lower-energy horizontal p state (denoted as the Pb_{p(xy)} state, corresponding to the CB1 state) and the higher-energy vertical p state (denoted as the Pb_{p(z)} state, corresponding to the CB2 state), due to the creation of the crystal field in the lattice. The unique advantage of the band-resolved optical constant analysis technique allows us to resolve the individual optical transition process to rank the contribution of each set of the occupied band and unoccupied band at each k point by projecting the predominant occupied (or unoccupied) electronic structures participating in these optical transition processes. The detailed procedures of projecting the predominant occupied or unoccupied electronic structures are shown in the ESI.† Four types of predominant optical transition processes at the Γ point, T1, T2, T3, and T4, are obtained, which are mainly responsible for the observed optical absorption at four different energies of Fig. 1(d) respectively, according to the weighting scheme in egn (2). Fig. 3(b) shows the orbital densities related to the four predominant optical transition processes T1-T4, which are mainly resulted from the states between two occupied states of VB1 and VB2 and two unoccupied states of CB1 and CB2 in the visible-light absorption region. It is clearly seen that the VB1 (σ^*) state consists of spherical-shaped s orbitals of Pb atoms and dumbbell-shaped p orbitals of I atoms along the Pb-I bond with a nodal plane. By contrast, the VB2 (I_{p(nb)}) state consists of donut-shaped orbitals of I atoms resulted from the degenerate p orbitals perpendicular to the Pb-I bonds. For the unoccupied states, the donut-shaped orbitals of Pb atoms that resulted from the mixing of degenerate p_x and p_y orbitals correspond to the CB1 ($Pb_{p(xy)}$) state, whereas the dumbbell-shaped p orbitals of Pb atoms correspond to the CB2 ($Pb_{p(z)}$) state, as a result of the MA cations aligned along the z direction. The optical transitions of T1 and T2 at lower energies mainly result from the same occupied states VB1 to the different unoccupied states CB1 and CB2, respectively. By contrast, the optical transitions of T3 and T4 at higher energies mainly result from another type of occupied state VB2 to the different unoccupied states CB1 and CB2, respectively. It is worth noting that the density plots in Fig. 2 correspond to the summation of the total contributions of all the allowed optical transition processes at four different energies (including all k points), while the density plots in Fig. 3(b) correspond to predominant transitions only at the individual k point (for example: Γ point) through a "bandresolved" partial summing strategy. By considering all the allowed optical transitions along the k points at each photon energy, Fig. 4(a) shows the relative ratios of the four types of optical transition processes T1-T4 as a function of photon energies ranging from NIR-Vis-UV absorption regions. It is found that T1 and T2 are the predominant optical transition processes in the lower energy range between 1.5 and 2.5 eV, where the contribution of T1 is gradually decreased while the contribution of T2 is increased with increasing energy. In the intermediate energy range between 2.5 and 3.3 eV, all these four types of optical transitions can be found, where T3 and T4 optical transition processes are gradually enhanced with increasing energies, accompanied by decreased ratios of T1

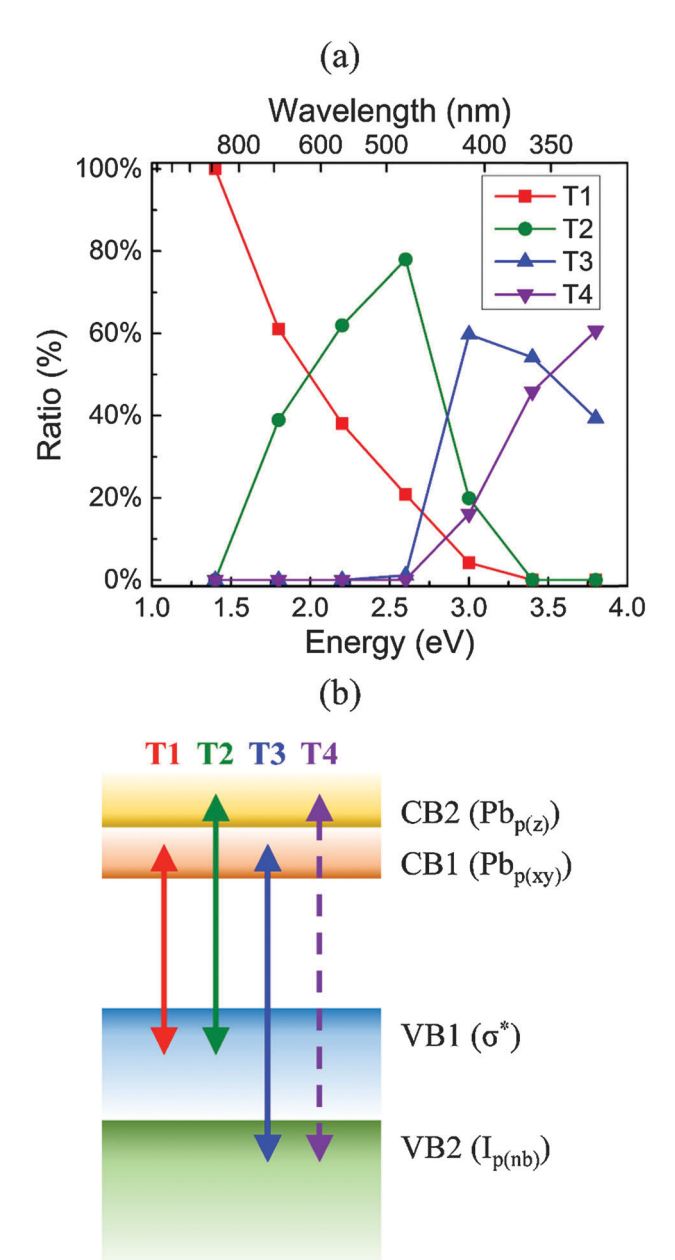


Fig. 4 (a) The ratios of four predominant transitions T1, T2, T3 and T4 ranging from NIR-Vis-UV absorption regions. (b) The corresponding schematic plot of the optical transition mechanism of polar MAPbI₃.

and T2. At the energies higher than 3.5 eV, only T3 and T4 optical transition processes become dominant and the ratio of T4 is increased with increasing energy. Fig. 4(b) shows the schematic band diagram and optical transition processes of the polar MAPbI₃ perovskite material. Optical transitions of polar MAPbI₃ mainly occur between two occupied (VB1, VB2) bands and two unoccupied bands (CB1, CB2) near the visible-light region and can thus be categorized into four types of optical transition processes T1, T2, T3 and T4 as we discussed above. The band-resolved optical constant analysis technique, to obtain the individual optical transition process at each k point or at each incident photon energy, thus allows us to reveal the

most important optical transition processes resulting from the atoms and orbitals at valence and conduction bands for understanding the light harvesting mechanism in perovskite materials.

Typically, MA cations in perovskite MAPbI₃ exhibit disorder in their orientations at room temperature, arising from enough thermal energy to overcome the activation energy for the rotational motion of MA cations within the lead tri-iodide framework. 36,37 Accordingly, the perovskite MAPbI₃ exhibits almost nonpolar behavior at room temperature due to the cancellation of electric dipole moments created by MA cations. 38-41 Fig. 5(a) shows the model of a non-polar MAPbI₃ (np-MAPbI₃) where there is no preferred orientation of MA cations within the lead tri-iodide framework of the perovskite crystal. The optical transition mechanism and corresponding optical constant density plots of occupied states and unoccupied states are also calculated (referring to the absorption spectrum of np-MAPbI₃ in the ESI†). In the occupied state, both the VB1' state with a higher energy corresponding to the antibonding state (σ^*) due to the orbital hybridizations of Pb and I and the VB2' state with a lower energy corresponding to the non-bonding state of $I_p(I_{p(nb)})$ are similar to the result obtained from the p-MAPbI₃ as shown above. However, the distinct energy separation between the $Pb_{p(xy)}$ state and the Pb_{p(z)} state as seen in the p-MAPbI₃ crystal has disappeared because there is no preferred orientation of MA cations. Therefore, a single unoccupied band CB', with the mixture of all types of p-character states of the Pb atom is found, resulting in a spherical shape orbital density as shown in Fig. 5(b). Two types of optical transition processes are responsible for the light-harvesting of the np-MAPbI₃ perovskite material; one is T1' with a lower absorption energy corresponding to the optical transition from VB1' to the CB' and the other is T2' with a

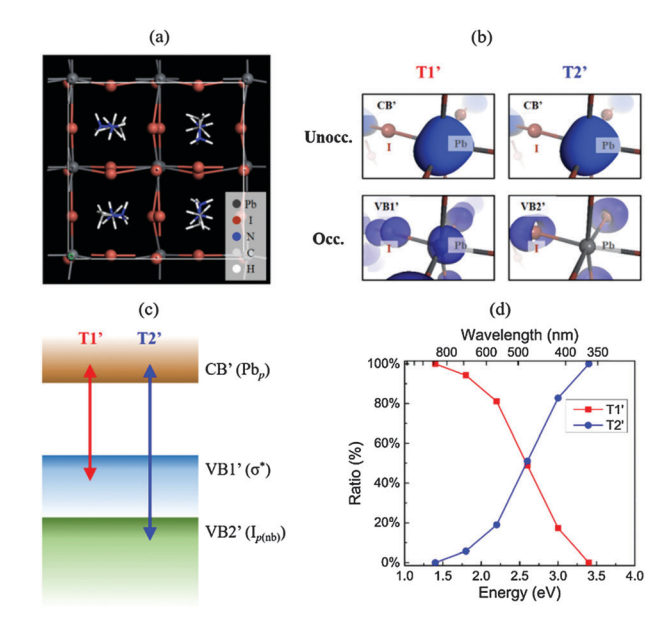


Fig. 5 (a) The model of non-polar MAPbl₃. (b) The corresponding 3D density plots of the predominant occupied and unoccupied states. (c) The schematic representation of the optical transition mechanism and (d) the ratios of the two predominant transitions of non-polar MAPbl₃, respectively.

higher absorption energy corresponding to the optical transition from VB2' to the CB' as shown schematically in Fig. 5(c). The relative ratios of the T1' and T2' transition processes as a function of photon energies are shown in Fig. 5(d). As the incident photon energy is lower than 2.5 eV, T1' is the dominant optical transition process while T2' becomes dominant when the energy is higher than 2.5 eV. According to the previous experimental result, 42-44 although the lower energy absorption peak (760 nm) is known to be mainly attributed to a direct band gap transition from the valence band maximum (VBM) to the conduction band minimum (CBM), the origin of the transition mechanism for the higher energy absorption peak (480 nm) is still not clear. It was found that the optical relaxation process corresponding to the absorption peak at 760 nm exhibited a shorter carrier lifetime, while the relaxation process corresponding to the absorption peak at 480 nm had a longer lifetime. Typically, photogenerated carriers at extended states may result in a shorter relaxation lifetime compared to those at localized states. Based on the bandresolved optical constant analysis technique, it is probable that the optical absorption of the lower energy absorption peak (760 nm) is mainly attributed to the optical transition of T1', corresponding to the optical transition from the VB1' (the antibonding (σ^*) to the CB' (Pb_p), where the antibonding (σ^*) VB1' is more extended within the lead tri-iodide framework. By contrast, the higher energy optical absorption peak (480 nm) is mainly resulting from the optical transition of T2', corresponding to the optical transition from the VB2' ($I_{p(nb)}$, the non-bonding state of I_p) to the CB' (Pb_p), where the non-bonding VB2' is mainly localized at the I atoms. Therefore, our calculation result based on the band-resolved optical constant analysis technique may provide the qualitative support for the experimental observation of different charge transfer behaviors at two distinct linear absorption peaks located at 480 nm and 760 nm according to the transient absorption spectroscopy data.9

Conclusions

In summary, we have demonstrated the wavelength-(or energy-)dependent optical transition mechanisms of perovskite materials using the first-principles calculations based on the band-resolved optical constant analysis technique. Based on the analyses, we are able to visualize and quantize the detailed wavelength-(or energy-)dependent optical transition processes to explain the light harvesting mechanism of perovskite-based photovoltaic materials. Through the band-resolved optical constant technique as shown above, the detailed optical transition processes of the perovskite materials can be clearly revealed, which may provide important information on the future design of perovskite-based photovoltaic materials for further improvement of light harvesting efficiencies and power conversion efficiencies.

Acknowledgements

This work was supported by Ministry of Science and Technology (MOST), Taiwan (Project No. 103-2119-M-002-021-MY3 and 102-2119-M-002-005), and Taiwan Consortium of Emergent Crystalline Materials (TCECM).

References

- 1 A. Kojima, K. Teshima, Y. Shirai and T. Miyasaka, J. Am. Chem. Soc., 2009, 131, 6050-6051.
- 2 M. M. Lee, J. Teuscher, T. Miyasaka, T. N. Murakami and H. J. Snaith, Science, 2012, 338, 643-647.
- 3 M. Z. Liu, M. B. Johnston and H. J. Snaith, *Nature*, 2013, **501**, 395-398.
- 4 S. Collavini, S. F. Volker and J. L. Delgado, Angew. Chem., Int. Ed., 2015, 54, 9757-9759.
- 5 S. De Wolf, J. Holovsky, S. J. Moon, P. Loper, B. Niesen, M. Ledinsky, F. J. Haug, J. H. Yum and C. Ballif, J. Phys. Chem. Lett., 2014, 5, 1035-1039.
- 6 J. Even, L. Pedesseau and C. Katan, J. Phys. Chem. C, 2014, **118**, 11566-11572.
- 7 S. D. Stranks, G. E. Eperon, G. Grancini, C. Menelaou, M. J. P. Alcocer, T. Leijtens, L. M. Herz, A. Petrozza and H. J. Snaith, Science, 2013, 342, 341-344.
- 8 C. Wehrenfennig, G. E. Eperon, M. B. Johnston, H. J. Snaith and L. M. Herz, Adv. Mater., 2014, 26, 1584-1589.
- 9 G. C. Xing, N. Mathews, S. Y. Sun, S. S. Lim, Y. M. Lam, M. Gratzel, S. Mhaisalkar and T. C. Sum, Science, 2013, 342, 344-347.
- 10 V. Roiati, S. Colella, G. Lerario, L. De Marco, A. Rizzo, A. Listorti and G. Gigli, Energy Environ. Sci., 2014, 7, 1889-1894.
- 11 Y. Yamada, T. Nakamura, M. Endo, A. Wakamiya and Y. Kanemitsu, J. Am. Chem. Soc., 2014, 136, 11610-11613.
- 12 P. Gao, M. Gratzel and M. K. Nazeeruddin, Energy Environ. Sci., 2014, 7, 2448-2463.
- 13 Z. G. Xiao, C. Bi, Y. C. Shao, Q. F. Dong, Q. Wang, Y. B. Yuan, C. G. Wang, Y. L. Gao and J. S. Huang, Energy Environ. Sci., 2014, 7, 2619-2623.
- 14 N. J. Jeon, J. H. Noh, W. S. Yang, Y. C. Kim, S. Ryu, J. Seo and S. I. Seok, Nature, 2015, 517, 476-480.
- 15 S. J. Clark, M. D. Segall, C. J. Pickard, P. J. Hasnip, M. J. Probert, K. Refson and M. C. Payne, Z. Kristallogr., 2005, 220, 567-570.
- 16 J. P. Perdew, K. Burke and M. Ernzerhof, Phys. Rev. Lett., 1996, 77, 3865-3868.
- 17 D. Vanderbilt, Phys. Rev. B: Condens. Matter Mater. Phys., 1990, 41, 7892-7895.
- 18 H. J. Monkhorst and J. D. Pack, Phys. Rev. B: Condens. Matter Mater. Phys., 1976, 13, 5188-5192.
- 19 A. Navrotsky, Chem. Mater., 1998, 10, 2787-2793.
- 20 A. Amat, E. Mosconi, E. Ronca, C. Quarti, P. Umari, M. K. Nazeeruddin, M. Gratzel and F. De Angelis, Nano Lett., 2014, 14, 3608-3616.
- 21 M. T. Weller, P. Henry, O. Weber, A. Di Pumpo and T. Hansen, Chem. Commun., 2015, 51, 4180-4183.
- 22 T. Baikie, Y. N. Fang, J. M. Kadro, M. Schreyer, F. X. Wei, S. G. Mhaisalkar, M. Graetzel and T. J. White, J. Mater. Chem. A, 2013, 1, 5628-5641.
- 23 Y. P. He and G. Galli, Chem. Mater., 2014, 26, 5394-5400.

- 24 P. Umari, E. Mosconi and F. De Angelis, Sci. Rep., 2014, 4, 4467.
- 25 G. Giorgi, J. I. Fujisawa, H. Segawa and K. Yamashita, J. Phys. Chem. C, 2014, 118, 12176–12183.
- 26 H. S. Kim, C. R. Lee, J. H. Im, K. B. Lee, T. Moehl, A. Marchioro, S. J. Moon, R. Humphry-Baker, J. H. Yum, J. E. Moser, M. Gratzel and N. G. Park, Sci. Rep., 2012, 2, 591.
- 27 J. H. Noh, S. H. Im, J. H. Heo, T. N. Mandal and S. I. Seok, Nano Lett., 2013, 13, 1764–1769.
- 28 G. E. Eperon, S. D. Stranks, C. Menelaou, M. B. Johnston, L. M. Herz and H. J. Snaith, *Energy Environ. Sci.*, 2014, 7, 982–988.
- 29 J. S. Toll, Phys. Rev., 1956, 104, 1760-1770.
- 30 N. J. Jeon, J. H. Noh, Y. C. Kim, W. S. Yang, S. Ryu and S. Il Seol, *Nat. Mater.*, 2014, 13, 897–903.
- 31 S. Colella, E. Mosconi, P. Fedeli, A. Listorti, F. Gazza, F. Orlandi, P. Ferro, T. Besagni, A. Rizzo, G. Calestani, G. Gigli, F. De Angelis and R. Mosca, *Chem. Mater.*, 2013, 25, 4613–4618.
- 32 N. Pellet, P. Gao, G. Gregori, T. Y. Yang, M. K. Nazeeruddin, J. Maier and M. Gratzel, Angew. Chem., Int. Ed., 2014, 53, 3151–3157.
- 33 M. H. Lee, C. H. Yang and J. H. Jan, *Phys. Rev. B: Condens. Matter Mater. Phys.*, 2004, **70**, 235110.
- 34 T. Tamura, S. Ishibashi, S. Tanaka, M. Kohyama and M. H. Lee, *Phys. Rev. B: Condens. Matter Mater. Phys.*, 2008, 77, 085207.

- 35 C. W. Chen, M. H. Lee and Y. T. Lin, Appl. Phys. Lett., 2006, 89, 223105.
- 36 J. H. Lee, N. C. Bristowe, P. D. Bristowe and A. K. Cheetham, Chem. Commun., 2015, 51, 6434–6437.
- 37 J. M. Frost, K. T. Butler, F. Brivio, C. H. Hendon, M. van Schilfgaarde and A. Walsh, *Nano Lett.*, 2014, 14, 2584–2590.
- 38 R. E. Wasylishen, O. Knop and J. B. Macdonald, *Solid State Commun.*, 1985, **56**, 581–582.
- 39 Y. Kawamura, H. Mashiyama and K. Hasebe, *J. Phys. Soc. Jpn.*, 2002, **71**, 1694–1697.
- 40 A. M. A. Leguy, J. M. Frost, A. P. McMahon, V. G. Sakai, W. Kochelmann, C. H. Law, X. E. Li, F. Foglia, A. Walsh, B. C. O'Regan, J. Nelson, J. T. Cabral and P. R. F. Barnes, *Nat. Commun.*, 2015, 6, 7124.
- 41 M. T. Weller, O. J. Weber, P. F. Henry, A. M. Di Pumpo and T. C. Hansen, *Chem. Commun.*, 2015, **51**, 4180–4183.
- 42 T. B. Song, Q. Chen, H. P. Zhou, C. Y. Jiang, H. H. Wang, Y. Yang, Y. S. Liu, J. B. You and Y. Yang, *J. Mater. Chem. A*, 2015, 3, 9032–9050.
- 43 W. G. Kong, Z. Y. Ye, Z. Qi, B. P. Zhang, M. Wang, A. Rahimi-Iman and H. Z. Wu, *Phys. Chem. Chem. Phys.*, 2015, 17, 16405–16411.
- 44 B. J. Foley, D. L. Marlowe, K. Y. Sun, W. A. Saidi, L. Scudiero, M. C. Gupta and J. J. Choi, *Appl. Phys. Lett.*, 2015, **106**, 243904.